



## Ruddlesden-Popper phases $\text{Sr}_3\text{Ni}_{2-x}\text{Al}_x\text{O}_{7-\delta}$ and some doped derivatives: Synthesis, oxygen nonstoichiometry and electrical properties

Inga M. Kharlamova<sup>a</sup>, Leonid V. Makhnach<sup>b</sup>, Alexandra E. Usenka<sup>b,\*</sup>, Alexander S. Lyakhov<sup>c</sup>, Ludmila S. Ivashkevich<sup>c</sup>, Vladimir V. Pankov<sup>b</sup>

<sup>a</sup> A. V. Luikov Heat and Mass Transfer Institute, National Academy of Sciences of Belarus, P. Brovka Str 15., 220072 Minsk, Belarus

<sup>b</sup> Belarusian State University, Nezalezhnastsi avenue 4, 220050 Minsk, Belarus

<sup>c</sup> Research Institute for Physical Chemical Problems of the Belarusian State University, Leningradskaya Str. 14, 220006 Minsk, Belarus



### ARTICLE INFO

#### Keywords:

Perovskite  
Ruddlesden–Popper structure  
Oxygen nonstoichiometry  
Specific electrical resistivity  
The Seebeck coefficient

### ABSTRACT

The Ruddlesden-Popper phases  $\text{Sr}_3\text{Ni}_{2-x}\text{Al}_x\text{O}_{7-\delta}$  ( $0.5 < x \leq 0.75$ ) were synthesized in the system Sr–Al–Ni–O for the first time. They show 2P/RS structure, in which two perovskite layers (P) are stacked in between rock-salt layers (RS). The composition  $\text{Sr}_3\text{Ni}_{2-x}\text{Al}_x\text{O}_{7-\delta}$  with  $x = 0.5$  was stabilized by partial substitution of  $\text{Sr}^{2+}$  for  $\text{Ba}^{2+}$  to give  $\text{Sr}_{2.8}\text{Ba}_{0.2}\text{Ni}_{1.5}\text{Al}_{0.5}\text{O}_{7-\delta}$ . This substitution allowed to reduce the synthesis duration and to lower its temperature. The study of specific electrical resistivity of  $\text{Sr}_3\text{Ni}_{2-x}\text{Al}_x\text{O}_{7-\delta}$  ( $0.5 < x \leq 0.75$ ) and  $\text{Sr}_{2.8}\text{Ba}_{0.2}\text{Ni}_{1.5}\text{Al}_{0.5}\text{O}_{7-\delta}$  ( $x = 0.5$ ) showed that it decreased with decreasing aluminum content. The specific resistivity of yttrium-modified phases  $\text{Sr}_{2.8-y}\text{Y}_y\text{Ba}_{0.2}\text{Ni}_{1.5}\text{Al}_{0.5}\text{O}_{7-\delta}$  was found to decrease with increasing  $y$  and reaches a minimum value for  $y = 0.1$ . Oxygen nonstoichiometry of limiting representatives in single phase range  $0.5 < x \leq 0.75$  was estimated by iodometric titration at 20 °C, which gave the oxygen deficiency  $\delta$  of 1.02 ( $x = 0.75$ ) and 0.78 ( $x = 0.5$ ), showing the decrease of  $\delta$  with decreasing aluminum content. The temperature range of semiconductor-to-metal transition (350–450 °C) was determined by thermal analysis and electrical measurements. All synthesized compounds were analyzed by X-ray powder diffraction for identification of crystalline phases.

### 1. Introduction

A large group of layered complex oxides  $\text{Sr}_3\text{M}_2\text{O}_{7-\delta}$  ( $\delta \geq 0$ ), where M is Ti [1], Fe [2], Co [3], Mn [4] and other 3d- and 4d-elements [5–7], is well-known due to their good transport, electrochemical, magnetic, catalytic properties and *etc.* These oxides belong to the Ruddlesden-Popper phase with 2P/RS structure, in which two perovskite layers (P) are stacked in between rock-salt layers (RS). The Ruddlesden-Popper-structured oxides are promising for application in different areas of industry, in particular energy production and information technology. Scientific importance and application fields of new synthesized compounds  $\text{Sr}_3\text{M}_2\text{O}_7$  will expand.

In [8] Z. Zhang et al. synthesized  $\text{La}_3\text{Ni}_2\text{O}_7$  at high oxygen pressure. M.A. Bobina et al. [9] established low solubility of strontium in this oxide. According to [9–11],  $\text{Sr}_3\text{Ni}_2\text{O}_7$  cannot be obtained in Sr–Ni–O system.

Our preliminary investigation showed that introduction of  $\text{Al}^{3+}$  in nickel sublattice promoted the formation of oxygen deficient 2P/RS phase. Although it is well-known that the single phase  $\text{Sr}_3\text{Al}_2\text{O}_7$  does

not exist in Sr–Al–O system.

So, the aim of the present work was to synthesize stable solid solutions  $\text{Sr}_3(\text{Ni}, \text{Al})_2\text{O}_{7-\delta}$  with 2P/RS structure and to study their oxygen nonstoichiometry and electrical properties. In the course of the investigation, solid solutions  $(\text{Sr}, \text{Ba})_3(\text{Ni}, \text{Al})_2\text{O}_{7-\delta}$  and  $(\text{Sr}, \text{Ba}, \text{Y})_3(\text{Ni}, \text{Al})_2\text{O}_{7-\delta}$  were also synthesized and studied.

### 2. Experimental

#### 2.1. Synthesis

Syntheses of complex oxides  $\text{Sr}_3(\text{Ni}, \text{Al})_2\text{O}_{7-\delta}$ ,  $(\text{Sr}, \text{Ba})_3(\text{Ni}, \text{Al})_2\text{O}_{7-\delta}$ , and  $(\text{Sr}, \text{Ba}, \text{Y})_3(\text{Ni}, \text{Al})_2\text{O}_{7-\delta}$  were carried out by the standard solid state reactions. Reagent grade nitrates  $\text{Sr}(\text{NO}_3)_2$ ,  $\text{Ni}(\text{NO}_3)_2 \cdot 6\text{H}_2\text{O}$ ,  $\text{Al}(\text{NO}_3)_3 \cdot 9\text{H}_2\text{O}$ ,  $\text{Ba}(\text{NO}_3)_2$ , and  $\text{Y}(\text{NO}_3)_3 \cdot 6\text{H}_2\text{O}$  were used as starting materials. Some details of the syntheses are described in Subsection 3.1.

\* Corresponding author at: Chemical Department of Belarusian State University, Leningradskaya Str. 14, 220030 Minsk, Belarus.

E-mail addresses: [alexusenka@gmail.com](mailto:alexusenka@gmail.com), [usenka@bsu.by](mailto:usenka@bsu.by) (A.E. Usenka).

## 2.2. Analytical procedures

The samples were investigated using powder X-ray diffraction (XRD) on an Empyrean diffractometer (PANalytical, Netherlands) at room temperature (CuK $\alpha$  radiation,  $\lambda = 1.5418 \text{ \AA}$ ).

The oxygen content of single-phase powders was determined by iodometric titration technique at a temperature of 20 °C. For iodometric titration, 50–80 mg of each sample was dissolved in a solution, containing 10 ml of 1 N potassium iodide and 10 ml of diluted (1:2) hydrochloric acid. The iodine formed was titrated against a standard 0.02 N solution of sodium thiosulfate.

Temperature variation of oxygen index was studied by coulometric titration with a multifunctional solid electrolyte device OXYLYT™ (GmbH SensoTech, Germany) over a temperature cycle 20–900–20 °C. The partial pressure of oxygen in flowing gas (Ar) was arbitrarily fixed at 49 Pa. Air was used as a comparison gas. The considered dependences were titration current ( $I$ ) and oxygen index vs. time ( $t$ ) and temperature ( $T$ ). The operation regimes of OXYLYT™ and its construction have been reviewed in [12] in detail. Here, it should be noted that the deviation of titration current ( $I$ ), being take place at any oxygen exchange of sample, from the base current value ( $I_{base}$ ), being correspond to fixed partial pressure of O<sub>2</sub> in flowing gas Ar, allows to calculate the mass change of oxygen according to Faraday's law:

$$\Delta m_{O_2} = \frac{M_{O_2}}{F \times z} \times \int_{t_1}^{t_2} (I_{base} - I) dt = \frac{32}{96485 \times 4} \times \int_{t_1}^{t_2} (I_{base} - I) dt \quad (1)$$

Thermal analysis was performed on a Netzsch STA429 thermo-analyzer, in a temperature range of 20–900 °C in nitrogen and air flows, using alumina crucibles. Thermogravimetric (TG) curves were obtained at heating rate 5 °C·min<sup>-1</sup> and gas flow rate 5 l·h<sup>-1</sup>.

## 2.3. Electrical measurements

Samples for electrical conductivity measurements were hydrostatically pressed at 400–600 MPa to form parallelepipeds with dimensions 10 × 4 × 4 mm<sup>3</sup>, and sintered at 1250–1300 °C for 20 h in oxygen flow. Specific electrical resistivity ( $\rho$ ) of samples was measured using a standard DC four-point method using double-sided platinum-rhodium electrodes. The dependence of specific electrical resistivity on temperature [ $\rho(T)$ ] was registered at heating/cooling rate of 2.6 °C·min<sup>-1</sup> in air and in oxygen atmosphere.

To establish the influence of temperature as well as atmosphere conditions on electrical properties of the samples,  $\ln \sigma(\text{Ohm}^{-1}\cdot\text{m}^{-1})$  vs. 1000/T(K) was plotted and the effective activation energy of conduction ( $E_a$ ) was estimated according to the Arrhenius Eqs. (2) and (2'):

$$\sigma = \sigma_0 \times \exp\left(-\frac{E_a}{RT}\right) \quad (2)$$

$$\ln \sigma = \ln \sigma_0 - \frac{E_a}{R} \frac{1}{T} \quad (2')$$

where  $\sigma$  is conductivity, or specific conductance (Ohm<sup>-1</sup>·m<sup>-1</sup>),  $\sigma_0$  – pre-exponential factor (Ohm<sup>-1</sup>·m<sup>-1</sup>),  $R$  – universal gas constant (8.314 J·mole<sup>-1</sup>·K<sup>-1</sup>).

In the present work, we analyzed simplified Arrhenius Eqs. (2) and (2') without any reference to hopping or semiconductor model of the samples conduction. The coefficient ( $-E_a/R$ ) was calculated by regression analysis using *Origin 7.0 SRO* software package (OriginLab. Corporation, Northampton, MA, USA). The final value of  $E_a$  was expressed in electron-volt units.

Coefficient of thermal electromotive force (EMF) or the Seebeck coefficient ( $\alpha$ ) was determined in air with respect to silver and subsequent conversion to microvolt units (with respect to lead). Temperature gradient between hot and cold ends of each sample was 10–15 °C.

## 3. Results and discussion

### 3.1. Synthesis and XRD study

According to [9–11], the oxide with the exact composition Sr<sub>3</sub>Ni<sub>2</sub>O<sub>7</sub> cannot be obtained due to the fact that the oxidation state +4 is not typical of nickel ions. Some Ruddlesden-Popper phases show exact composition Sr<sub>3</sub>M<sub>2</sub>O<sub>7</sub>, as in the case of Sr<sub>3</sub>Ti<sub>2</sub>O<sub>7</sub> [13, 14], which became a traditional example of Ruddlesden-Popper compounds Sr<sub>3</sub>M<sub>2</sub>O<sub>7</sub> (titanium ion is in oxidation state +4). Other Ruddlesden-Popper phases, such as Sr<sub>3</sub>Fe<sub>2</sub>O<sub>7- $\delta$</sub>  and Sr<sub>3</sub>Co<sub>2</sub>O<sub>7- $\delta$</sub> , revealed large oxygen deficiency, because cobalt and iron ions do not attain oxidation state +4. For example, in Sr<sub>3</sub>Co<sub>2</sub>O<sub>7- $\delta$</sub>  [3], the oxygen deficiency  $\delta$  was found to be close to 1.

It was found in the course of the present investigations, that the introduction of Al<sup>3+</sup> in Sr–Ni–O system is the factor, stabilizing oxygen deficient 2P/RS-structure. The investigation showed that single phase oxides Sr<sub>3</sub>Ni<sub>2- $x$</sub> Al <sub>$x$</sub> O<sub>7- $\delta$</sub>  could be synthesized by partial substitution of Ni-sites by Al<sup>3+</sup> only in the range 0.5 <  $x$  ≤ 0.75. Synthesis of such phases were prepared with a step  $\Delta x = 0.05$  by the following way. An aqueous solution of starting nitrates, taken in corresponding ratio, was evaporated by slow heating from 20 °C to 350 °C. The obtained mixture of solid products was grinded and sintered at 750 °C for 5 h to complete decomposition of nitrates. As a result, fine powder oxide was formed. Subsequent sintering of the powder at 1100–1150 °C in oxygen-rich atmosphere enhanced the reaction between oxides to form precursors. The precursors were grinded and sintered at 1300–1320 °C for 30 h in oxygen flow to give the resulting sample. As showed XRD powder patterns of the obtained samples with 0.5 <  $x$  ≤ 0.75, all they are single phases Sr<sub>3</sub>Ni<sub>2- $x$</sub> Al <sub>$x$</sub> O<sub>7- $\delta$</sub>  with Ruddlesden-Popper 2P/RS-structure, crystallizing in the tetragonal space group *I4/mmm*. Fig. 1a shows XRD powder pattern of Sr<sub>3</sub>Ni<sub>1.25</sub>Al<sub>0.75</sub>O<sub>7- $\delta$</sub> , being the representative with the highest aluminum content. Its unit cell dimensions was found to be  $a = 3.8198(2) \text{ \AA}$  and  $c = 20.325(2) \text{ \AA}$ .

The samples, synthesized for  $x > 0.75$  and  $x \leq 0.5$ , were found to be multiphase. So, according to XRD powder data, the sample with  $x = 0.8$  contained a small amount of Sr<sub>3</sub>Al<sub>2</sub>O<sub>6</sub>. Oxides NiO and SrO were observed in the sample obtained for  $x < 0.5$ , and very small amount of these oxides was found in the sample with  $x = 0.5$ . To facilitate single phase synthesis for  $x = 0.5$ , partial substitution of Sr-sites by Ba<sup>2+</sup> was performed. Final stage of the sample synthesis (*i.e.* formation of 2P/RS-structure) could be performed by sintering the sample at 1270–1280 °C for 18–20 h. As a result, single phase

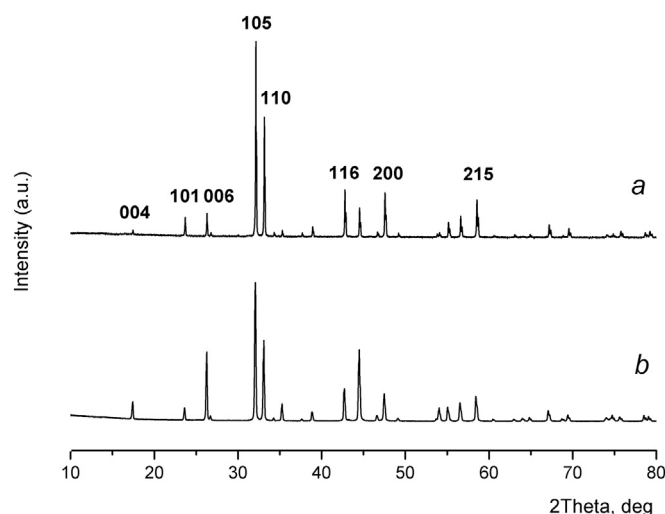


Fig. 1. XRD powder patterns of the samples with nominal compositions Sr<sub>3</sub>Ni<sub>1.25</sub>Al<sub>0.75</sub>O<sub>7- $\delta$</sub>  (a) and Sr<sub>2.8</sub>Ba<sub>0.2</sub>Ni<sub>1.5</sub>Al<sub>0.5</sub>O<sub>7- $\delta$</sub>  (b).

**Table 1**Results of iodometric titration<sup>a</sup> of  $\text{Sr}_3\text{Ni}_{1.25}\text{Al}_{0.75}\text{O}_{7-\delta}$  and  $\text{Sr}_{2.8}\text{Ba}_{0.2}\text{Ni}_{1.5}\text{Al}_{0.5}\text{O}_{7-\delta}$  for definition of oxygen deficiency ( $\delta$ ).

Nominal composition	Range of obtained $\delta$	Average $\delta$	Specified formula	Oxidation state of nickel ions
$\text{Sr}_3\text{Ni}_{1.25}\text{Al}_{0.75}\text{O}_{7-\delta}$	0.96–1.05	1.02	$\text{Sr}_3\text{Ni}_{1.25}\text{Al}_{0.75}\text{O}_{5.98}$	+2.97
$\text{Sr}_{2.8}\text{Ba}_{0.2}\text{Ni}_{1.5}\text{Al}_{0.5}\text{O}_{7-\delta}$	0.76–0.79	0.78	$\text{Sr}_{2.8}\text{Ba}_{0.2}\text{Ni}_{1.5}\text{Al}_{0.5}\text{O}_{6.22}$	+3.29

<sup>a</sup> Titration procedure was repeated for four samples of the same nominal composition, and each sample was tested three times to reduce random errors in  $\delta$ .

$\text{Sr}_{2.8}\text{Ba}_{0.2}\text{Ni}_{1.5}\text{Al}_{0.5}\text{O}_{7-\delta}$  was obtained. Thus, in comparison with the synthesis of  $\text{Sr}_3\text{Ni}_{2-x}\text{Al}_x\text{O}_{7-\delta}$ , the introduction of  $\text{Ba}^{2+}$  decreased duration of final stage of the synthesis by  $\sim 1/3$  and somewhat lowered its temperature.

### 3.2. Oxygen nonstoichiometry

Oxygen nonstoichiometry was estimated by iodometric titration, coulometric measurements and thermogravimetry.

#### 3.2.1. Iodometric titration

Iodometric titration was carried out for  $\text{Sr}_3\text{Ni}_{1.25}\text{Al}_{0.75}\text{O}_{7-\delta}$  and barium-doped  $\text{Sr}_{2.8}\text{Ba}_{0.2}\text{Ni}_{1.5}\text{Al}_{0.5}\text{O}_{7-\delta}$ , being representatives with limit  $x$  values of single phase range  $0.5 \leq x \leq 0.75$ . In order to increase accuracy of oxygen index estimation, the samples of the same composition from different batches were analyzed. The obtained values of oxygen deficiency ( $\delta$ ) and calculated from them specified formulae together with oxidation state of nickel ions are given in Table 1.

As follows from Table 1, two investigated single phase representatives are oxygen-deficient, the representative with  $x = 0.75$  being more oxygen deficient compared to that with  $x = 0.5$ . Oxidation state of nickel ions is close to +3 and somewhat increases with decreasing  $x$ . We believe that the decrease of aluminum content lowers oxygen deficiency for all compositions in the range  $0.5 \leq x \leq 0.75$ .

#### 3.2.2. Coulometric measurements

Curves of titration current and oxygen index of the sample  $\text{Sr}_3\text{Ni}_{1.25}\text{Al}_{0.75}\text{O}_{5.98}$ , heated to 900°C in argon flow with low partial pressure of  $\text{O}_2$ , are shown in Fig. 2. According to the curve shape, the sample began to evolve oxygen at about 380°C and the value of oxygen index decreased to 5.63 at 900°C. When cooled, the sample absorbed  $\text{O}_2$ . To return the initial value of oxygen index, the oxide should be cooled in oxygen-rich flow.

#### 3.2.3. Thermogravimetric analysis

TG curves for  $\text{Sr}_3\text{Ni}_{1.25}\text{Al}_{0.75}\text{O}_{5.98}$  were obtained at heating from 20°C to 900°C in nitrogen and air flows (Fig. 3). Two ranges of different temperature behaviour of the sample in the two flows can be seen in Fig. 3. In the first range of 20–450°C, the curves are almost similar, but

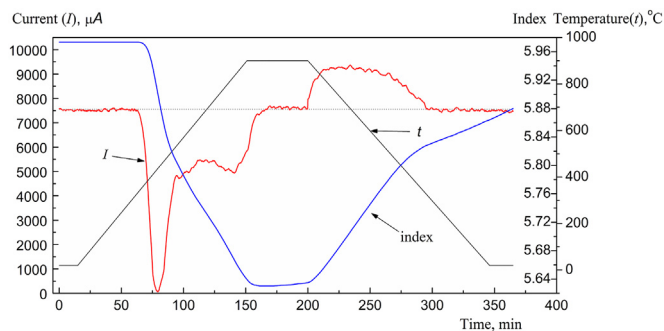


**Fig. 2.** Coulometric titration curve (red) and oxygen index (blue) of  $\text{Sr}_3\text{Ni}_{1.25}\text{Al}_{0.75}\text{O}_{5.98}$  in a temperature cycle 20–900–20 °C in argon flow (oxygen partial pressure 49 Pa, heating/cooling rate 6 °C·min<sup>-1</sup>). (For interpretation of the references to colour in this figure legend, the reader is referred to the web version of this article.)

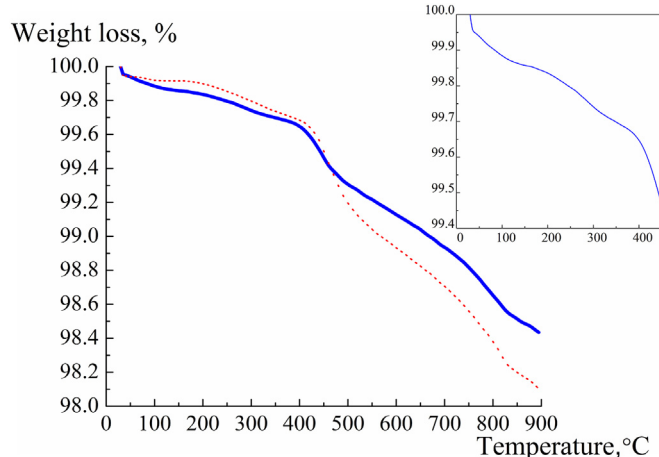


**Fig. 3.** TG curves of  $\text{Sr}_3\text{Ni}_{1.25}\text{Al}_{0.75}\text{O}_{5.98}$  recorded in nitrogen flow (red point line) and air flow (blue solid line) at heating rate of 5 °C·min<sup>-1</sup>. The insert presents an enlarged fragment of TG curve from 20 to 400 °C (in air flow). (For interpretation of the references to colour in this figure legend, the reader is referred to the web version of this article.)

they show different slope in the second range of 450–900°C. Above 400°C, the steepness of TG curves (*i.e.* intensity of the weight loss due to desorption of  $\text{O}_2$ ) depends on partial pressure of oxygen. Because desorption of  $\text{O}_2$  in oxygen-free flow should be more intensive than in air flow, the curve, recorded in nitrogen flow, shows a steeper slope in comparison with that in air flow, as it was expected.

Comparing the curves in Figs. 2 and 3, one can conclude that the weight loss below 400°C is not related to oxygen desorption. This follows from the absence of such a loss on coulometric titration curves and convergence of TG curves in appropriate temperature range. A steeper slope of TG curve in the range 20–100 °C (see the insert in Fig. 3) compared to 125–400 °C is caused by removal of water. It can be assumed that the weight loss in the range 100–450°C is related to the removal of water and OH-groups from hydrated  $\text{Sr}_3\text{Ni}_{1.25}\text{Al}_{0.75}\text{O}_5(\text{OH})_2 \cdot x\text{H}_2\text{O}$ , contained in  $\text{Sr}_3\text{Ni}_{1.25}\text{Al}_{0.75}\text{O}_{7-\delta}$  sample in a small amount. This assumption follows from the fact that TG curve, recorded for the investigated sample in air flow, is similar to that for hydrated  $\text{Sr}_3\text{Co}_2\text{O}_5(\text{OH})_2 \cdot x\text{H}_2\text{O}$  [15]. However, the weight loss of the latter in the range 20–400 °C ( $\sim 9\%$ ) was considerably greater than that of our sample ( $\sim 0.7\%$ ).

### 3.3. Electrical properties

It was established during the investigations that specific electrical resistivity  $\rho$  of the samples  $\text{Sr}_3\text{Ni}_{2-x}\text{Al}_x\text{O}_{7-\delta}$  at 20°C decreased from  $802.0 \times 10^{-3}$  Ohm·cm to  $20.5 \times 10^{-3}$  Ohm·cm with decreasing aluminum content from  $x = 0.75$  to  $x = 0.55$ , respectively. The value of  $\rho$  for barium-stabilized sample  $\text{Sr}_{2.8}\text{Ba}_{0.2}\text{Ni}_{1.5}\text{Al}_{0.5}\text{O}_{7-\delta}$  ( $x = 0.5$ ) was found to be  $18.2 \times 10^{-3}$  Ohm·cm.

For further decrease in specific resistivity,  $\text{Sr}_{2.8}\text{Ba}_{0.2}\text{Ni}_{1.5}\text{Al}_{0.5}\text{O}_{7-\delta}$  was doped by yttrium, with the substitution index of Sr-sites  $y \leq 0.1$ . For the obtained  $\text{Sr}_{2.8-y}\text{Y}_y\text{Ba}_{0.2}\text{Ni}_{1.5}\text{Al}_{0.5}\text{O}_{7-\delta}$ , the values of  $\rho$  continued to decrease with increasing  $y$  to give the lowest value  $\sim 5 \times 10^{-3}$  Ohm·cm for the sample with  $y = 0.1$ . Below  $\sim 400$ – $450$ °C, all yttrium-

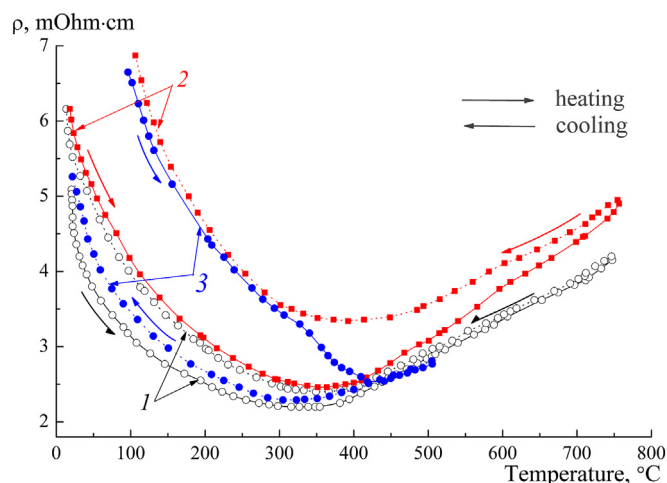


Fig. 4. Temperature dependence of specific electrical resistivity  $\rho$  of  $\text{Sr}_{2.7}\text{Y}_{0.1}\text{Ba}_{0.2}\text{Ni}_{1.5}\text{Al}_{0.5}\text{O}_{7-\delta}$ . 1 – the first cycle in oxygen flow; 2 – the second cycle in air flow; 3 – the third cycle in oxygen flow.

doped compounds behaved as semiconductors, and above  $450^\circ\text{C}$  they show the metal type of conductivity. Temperature dependences of  $\rho$  and the Seebeck coefficient  $\alpha$  for the sample  $\text{Sr}_{2.7}\text{Y}_{0.1}\text{Ba}_{0.2}\text{Ni}_{1.5}\text{Al}_{0.5}\text{O}_{7-\delta}$ , showing the highest conductivity, are depicted in Figs. 4 and 5, respectively. Temperature dependence of  $\rho$  was recorded in the range  $20\text{--}750^\circ\text{C}$  in three cycles of heating/cooling: the first and the third cycles were in oxygen flow, and the second one was in air flow.

The influence of oxygen nonstoichiometry on specific resistivity of  $\text{Sr}_{2.7}\text{Y}_{0.1}\text{Ba}_{0.2}\text{Ni}_{1.5}\text{Al}_{0.5}\text{O}_{7-\delta}$  and its conductive properties can be seen from Figs. 4 and 5. In the first cycle, the sample behaved as a semiconductor from  $20^\circ\text{C}$  to  $\sim 370^\circ\text{C}$ , and as a metal above  $370^\circ\text{C}$ . The cooling and heating curves  $\rho(T)$  of the cycle are nearly converged at  $\sim$

$750\text{--}450^\circ\text{C}$  and diverged below  $\sim 450^\circ\text{C}$ , the start point of heating being inconsistent with the end point of cooling. The above inconsistency is probably related to insufficient amount of absorbed oxygen at cooling as compared to desorbed oxygen at heating. The assumption may be confirmed by the values of the conductivity and activation energy of conduction  $E_a$ . One can see from Fig. 5a, that  $\ln\sigma$  at heating is higher than that at cooling when temperature is below  $\sim 400^\circ\text{C}$ . In the temperature range  $\sim 20\text{--}400^\circ\text{C}$ ,  $E_a$  at cooling ( $0.043\text{ eV}$ ) is higher than at heating ( $0.038\text{ eV}$ ). In the second cycle (in air flow), heating curve  $\rho(T)$  is close to cooling one of the first cycle from  $20^\circ\text{C}$  to  $\sim 420^\circ\text{C}$  (the temperature region where the sample did not desorb oxygen), the appropriate values of  $E_a$  coincide ( $0.043\text{ eV}$ ), and above  $420^\circ\text{C}$  (when the sample starts to evolve  $\text{O}_2$ ), these curves are diverged. Such a tendency is in agreement with the shape of TG curves (Fig. 3). At low oxygen pressure, TG curve is steeper than that in air flow due to more intensive oxygen desorption. Oxygen desorption in air, being more intensive than in oxygen flow, leads to increase in specific electrical resistivity/decrease of conductivity of the sample. Oxygen index at cooling did not reach the value obtained in oxygen flow, and the cooling curve  $\rho(T)$  of the second cycle was significantly higher than that for the first cycle. From comparison of Fig. 5a and b, it becomes obvious that activation energy of conductivity in the second cycle at cooling from  $\sim 330^\circ\text{C}$  to  $20^\circ\text{C}$  is higher than that for the first cycle too, i.e.  $0.063\text{ eV}$  vs.  $0.043\text{ eV}$ . The third cycle, performed in oxygen flow, allows to identify the range of oxygen absorption. So, the heating curve  $\rho(T)$  runs down abruptly from  $\sim 320^\circ\text{C}$  to  $\sim 420^\circ\text{C}$  and in the range  $420\text{--}500^\circ\text{C}$  becomes close to the curve for the first cycle. This indicates that the sample is saturated with oxygen, because absorption of  $\text{O}_2$  leads to increase in conductivity, and the tendency is confirmed by appropriate curves in Fig. 5c. The values of  $\ln\sigma$  and  $E_a$  became similar to those in the first cycle at cooling.

Summarizing the data on the electrical behavior, it is important to note that the temperature of semiconductor-to-metal transition shifts to lower values with a decrease in the specific resistivity of the oxide.

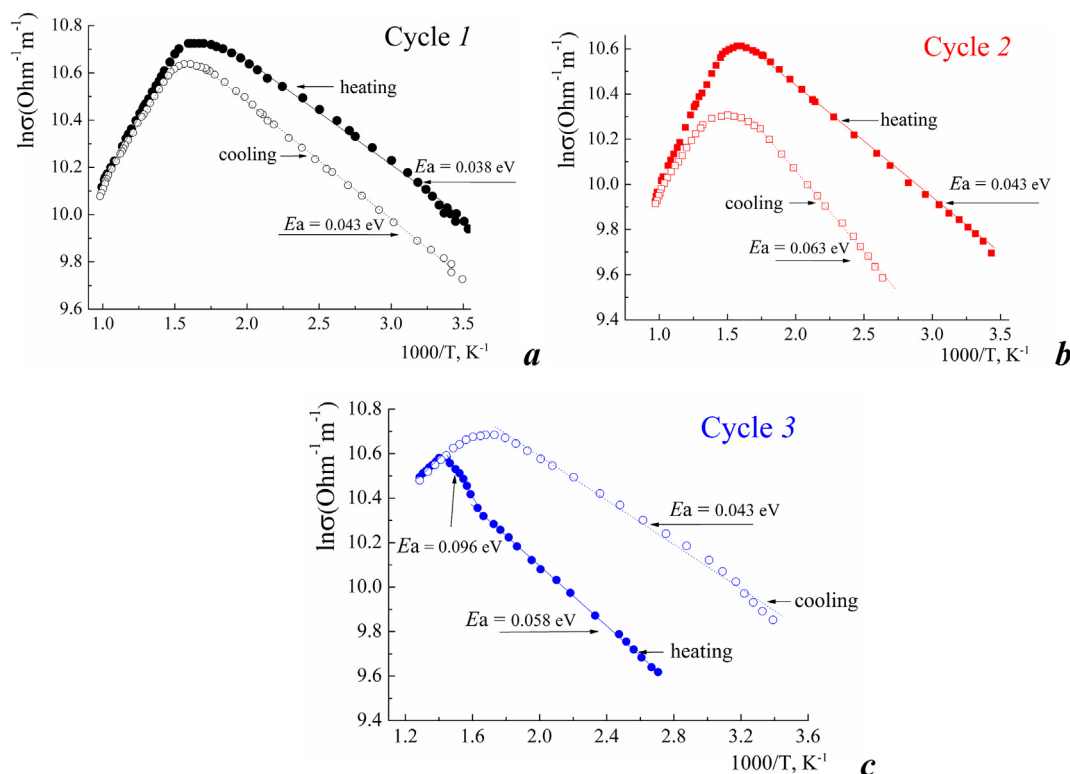


Fig. 5.  $\ln(\sigma(\text{Ohm}^{-1}\text{m}^{-1}))$  vs.  $1000/T(\text{K})$  for the sample  $\text{Sr}_{2.7}\text{Y}_{0.1}\text{Ba}_{0.2}\text{Ni}_{1.5}\text{Al}_{0.5}\text{O}_{7-\delta}$ . a – the first cycle in oxygen flow; b – the second cycle in air flow; c – the third cycle in oxygen flow.

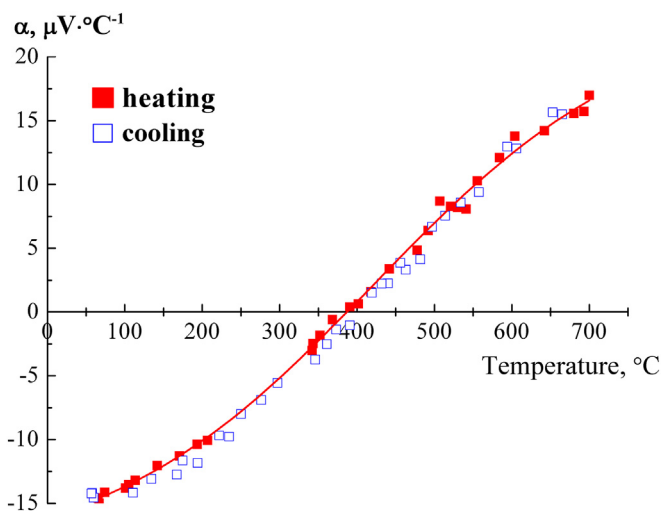


Fig. 6. Temperature dependence of the Seebeck coefficient  $\alpha$  for  $\text{Sr}_{2.7}\text{Y}_{0.1}\text{Ba}_{0.2}\text{Ni}_{1.5}\text{Al}_{0.5}\text{O}_{7-\delta}$  in air.

At temperatures 20–580°C in air, the Seebeck coefficient of  $\text{Sr}_{2.7}\text{Y}_{0.1}\text{Ba}_{0.2}\text{Ni}_{1.5}\text{Al}_{0.5}\text{O}_{7-\delta}$  is negative, and above  $\sim 390^\circ\text{C}$  it becomes positive (Fig. 6). Consequently, electro-transport properties of the oxide are determined by electrons below  $\sim 390^\circ\text{C}$  and by holes above  $\sim 390^\circ\text{C}$ . Because an increase in nickel and oxygen content resulted in increase in conductivity, these ions are the main suppliers of charge carriers, like other perovskite-like nickelates. Localization-delocalization of outer electrons and their redistribution between the ions influence on carrier mobility (electrons and holes) that results in a change of conductivity type.

It should be noted that the influence of mobile oxygen on conductivity of  $\text{La}_2\text{NiO}_{4+\delta}$  and  $\text{La}_{2-x}\text{Sr}_x\text{NiO}_{4-\delta}$  ( $x = 1.0\text{--}1.4$ ) at heating was discussed in works [16–19]. Their authors demonstrated the presence of anomalies in the oxygen desorption region of the temperature dependence of  $\rho$  of the nickelates, induced by the lattice oxygen. Interstitial oxygen in  $\text{La}_2\text{NiO}_{4+\delta}$  did not induce the anomalies. The absence of such anomalies in the temperature dependence of  $\rho$  of the aluminickelate under consideration may imply that mobile oxygen presents interstitial oxygen.

The structure of synthesized compounds  $\text{Sr}_3\text{Ni}_{2-x}\text{Al}_x\text{O}_{7-\delta}$ , being isotopic with oxide  $\text{La}_3\text{Ni}_2\text{O}_{7-\delta}$  [8], is shown in Fig. 7. According to [8],  $\text{La}_3\text{Ni}_2\text{O}_{7-\delta}$  contains two types of apical oxygen atoms in oxygen octahedrons: O(1) atoms link two  $\text{NiO}_2$  layers while O(2) atoms link LaO and  $\text{NiO}_2$  layers, i.e. O(2) links layers of rock salt and perovskite.

As a result of the reduction of  $\text{La}_3\text{Ni}_2\text{O}_{7.00}$  to  $\text{La}_3\text{Ni}_2\text{O}_{6.35}$ , the total oxygen loss was found to correspond to the loss of 65% of O(1) atoms. Taking into account this result for  $\text{La}_3\text{Ni}_2\text{O}_{7-\delta}$ , one would expect that oxygen deficient phase  $\text{Sr}_3\text{Ni}_{1.25}\text{Al}_{0.75}\text{O}_6$  does not contain O(1) atoms. The same assumption could be applied to  $\text{Sr}_3\text{Ni}_{1.5}\text{Al}_{0.5}\text{O}_{6+\gamma}$  ( $\text{Sr}_3\text{Ni}_{1.5}\text{Al}_{0.5}\text{O}_{7-\delta}$ ) and  $\text{Sr}_{2.8}\text{Ba}_{0.2}\text{Ni}_{1.5}\text{Al}_{0.5}\text{O}_{6+\gamma}$  ( $\gamma = 0.21\text{--}0.24$ ) oxides. But we think that there is a lack of experimental data to accept this assumption.

The oxygen  $\gamma$  is absorbed at cooling and occupies interstitial sites. It is the oxygen that demonstrates mobility in thermal cycles (for example, temperature dependence of specific resistivity  $\rho(T)$ ). However the composition  $\text{Sr}_3\text{Ni}_{1.25}\text{Al}_{0.75}\text{O}_{6.00}$  contains the same oxygen. Consequently, the oxygen deficient structure  $\text{Sr}_3\text{Ni}_{1.25}\text{Al}_{0.75}\text{O}_{6-\gamma}$  is formed at the synthesis temperature. Oxygen deficiency in the oxide can't be explained by absence of O(1) sites solely. Even if all the O(1) sites are empty one has to admit that some fraction of O(3) or O(2) sites isn't occupied to explain such a great deficiency of oxygen in  $\text{Sr}_3\text{Ni}_{1.25}\text{Al}_{0.75}\text{O}_{6-\gamma}$ . Formation of vacancies in O(2) sites for the Ruddlesden-Popper phase with  $n = 2$  (2P/RS) is improbable according to many investigations [20]. Consequently, the oxides

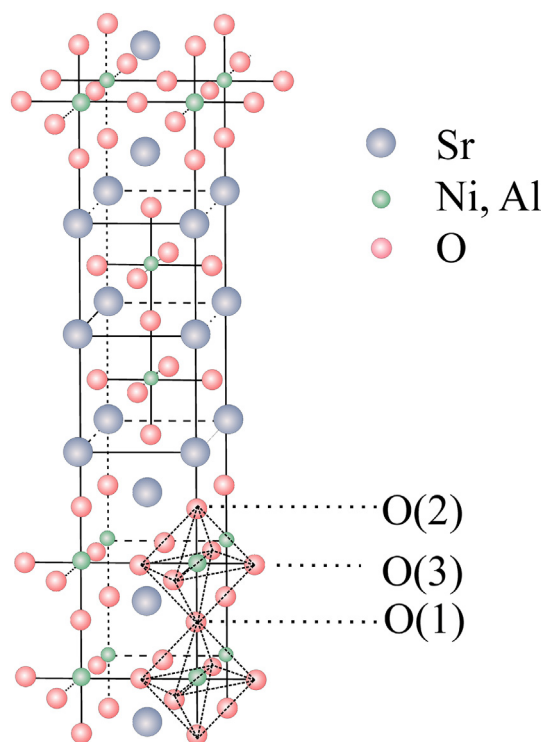


Fig. 7. The structure of  $\text{Sr}_3\text{Ni}_{2-x}\text{Al}_x\text{O}_{7-\delta}$  (adapted from [8]).

$\text{Sr}_3\text{Ni}_{1.25}\text{Al}_{0.75}\text{O}_{6-\gamma}$  with unoccupied O(1) as well as O(3) sites are formed at the synthesis temperature. But preliminary Rietveld refinement of XRD powder data didn't confirm complete absence of O(1) sites for  $\text{Sr}_3\text{Ni}_{1.25}\text{Al}_{0.25}\text{O}_{7-\delta}$ .

The role of atoms O(1), O(2) and O(3) in the formation of oxygen deficiency as well as their mobility in aluminickelates require additional experimental data, and these questions will be the topic of our future work.

#### 4. Conclusions

The aluminickelates  $\text{Sr}_3\text{Ni}_{2-x}\text{Al}_x\text{O}_{7-\delta}$  ( $0.5 < x \leq 0.75$ ) were synthesized in Sr–Ni–Al–O system. They crystallize in the tetragonal space group  $I4/mmm$  and belong to the Ruddlesden-Popper phase 2P/RS, in which two perovskite layers (P) stacked in between rock-salt layers (RS). The compounds are oxygen deficient, with  $\delta = 0.78\text{--}1.02$  according to the iodometric titration technique. The partial substitution of  $\text{Sr}^{2+}$  by  $\text{Ba}^{2+}$  allows to optimize the synthesis conditions of the most conductive composition  $\text{Sr}_3\text{Ni}_{1.5}\text{Al}_{0.5}\text{O}_{7-\delta}$ , namely sintering in oxygen flow at  $1270\text{--}1280^\circ\text{C}$  for 18–20 h is sufficient to form 2P/RS phase  $\text{Sr}_{2.8}\text{Ba}_{0.2}\text{Ni}_{1.5}\text{Al}_{0.5}\text{O}_{7-\delta}$ . At the synthesis temperatures, the aluminickelates have oxygen deficient structure. When cooling, they are saturated with mobile interstitial oxygen, the temperature range of saturation being of about  $300\text{--}450^\circ\text{C}$ .

The specific electrical resistivity of the samples  $\text{Sr}_3\text{Ni}_{2-x}\text{Al}_x\text{O}_{7-\delta}$  at  $20^\circ\text{C}$  decreases with decreasing  $x$ , namely from  $802.0 \times 10^{-3}$  Ohm-cm for  $x = 0.75$  to  $20.5 \times 10^{-3}$  Ohm-cm for  $x = 0.55$ . The substitution of Sr-sites by Y of the samples  $\text{Sr}_{2.8}\text{Ba}_{0.2}\text{Ni}_{1.5}\text{Al}_{0.5}\text{O}_{7-\delta}$  leads to a further decrease in the specific electrical resistivity. All the synthesized samples are semiconductors of  $n$ -type at temperatures from  $20^\circ\text{C}$  to about  $350\text{--}450^\circ\text{C}$ , and they behave as metals above  $400\text{--}450^\circ\text{C}$ . The lower is specific electrical resistivity of the samples the lower is the temperature of their semiconductor-to-metal transition. One should expect that an increase in concentration of the mobile oxygen will result in considerable decrease in the specific resistivity of the aluminickelates. To reach high concentration of such oxygen, it is necessary to heat the samples

(300–450 °C) at high oxygen pressure of about 50–70 atm.

## Acknowledgements

This work was supported by the National Academy of Sciences of Belarus and the Ministry of Education of the Republic of Belarus (State Program of Scientific Investigations “Energetic Systems, Processes and Technologies”, state registration number 20161627, 2016–2018).

## References

- [1] I. Zvereva, I. German, Y.R. Smirnov, J. Choisnet, Evidence of Cr<sup>4+</sup> doping in Sr<sub>3</sub>Ti<sub>2</sub>O<sub>7</sub> from structural, optical and magnetic properties, *J. Mater. Sci. Lett.* 20 (2001) 127–130, <https://doi.org/10.1023/A:1006786119155>.
- [2] M. Matvejeff, M. Lehtimäki, A. Hirasa, Y.-H. Huang, H. Yamauchi, M. Karppinen, New water-containing phase derived from the Sr<sub>3</sub>Fe<sub>2</sub>O<sub>7.8</sub> phase of the Ruddlesden–Popper structure, *Chem. Mater.* 17 (2005) 2775–2779, <https://doi.org/10.1021/cm050106z>.
- [3] X.L. Wang, H. Sakurai, E. Takayama-Muromachi, Synthesis, structures, and magnetic properties of novel Ruddlesden–Popper homologous series Sr<sub>n+1</sub>Co<sub>n</sub>O<sub>3n+1</sub> (n = 1, 2, 3, 4, and ∞), *J. Appl. Phys.* 97 (2005) 10M519, <https://doi.org/10.1063/1.1855534>.
- [4] J.F. Mitchell, J.E. Millburn, M. Medarde, S. Short, J.D. Jorgensen, M.T. Fernández-Díaz, Sr<sub>3</sub>Mn<sub>2</sub>O<sub>7</sub>: Mn<sup>4+</sup> parent compound of the n = 2 layered CMR manganites, *J. Solid State Chem.* 141 (1998) 599–603, <https://doi.org/10.1006/jssc.1998.8026>.
- [5] E. Castillo-Martínez, M.Á. Alario-Franco, Revisiting the Sr–Cr(IV)–O system at high pressure and temperature with special reference to Sr<sub>3</sub>Cr<sub>2</sub>O<sub>7</sub>, *Solid State Sci.* 9 (2007) 564–573, <https://doi.org/10.1016/j.solidstatesciences.2007.02.008>.
- [6] M. Itoh, M. Shikano, H. Kawaji, T. Nakamura, Structural aspects on the variations of electric and magnetic properties of the layered compound system Sr<sub>n+1</sub>V<sub>n</sub>O<sub>3n+1-δ</sub> (n = 1, 2, 3, ∞), *Solid State Commun.* 80 (1991) 545–548, [https://doi.org/10.1016/0038-1098\(91\)90147-N](https://doi.org/10.1016/0038-1098(91)90147-N).
- [7] S. Kouno, N. Shirakawa, I. Nagai, N. Umeyama, K. Tokiwa, T. Watanabe, The synthesis and characterization of double-layered perovskite Sr<sub>3</sub>Mo<sub>2</sub>O<sub>7</sub>, *J. Phys. Soc. Jpn.* 76 (2007) 94706, <https://doi.org/10.1143/JPSJ.76.094706>.
- [8] Z. Zhang, M. Greenblatt, J.B. Goodenough, Synthesis, structure, and properties of the layered perovskite La<sub>3</sub>Ni<sub>2</sub>O<sub>7.8</sub>, *J. Solid State Chem.* 108 (1994) 402–409, <https://doi.org/10.1006/jssc.1994.1059>.
- [9] M.A. Bobina, N.A. Yakovleva, L.Y. Gavrilova, V.A. Cherepanov, Phase equilibria in the La–Sr–Ni–O system, *Russ. J. Phys. Chem.* 78 (8) (2004) 1340–1343.
- [10] M.A. Melkozerova, T.V. Aksenova, L.Y. Gavrilova, V.A. Cherepanov, Phase equilibria and the structure of individual phases in the Sr–Co–Ni–O system at 1100 °C in air, *Russ. J. Phys. Chem.* 79 (8) (2005) 1197–1202.
- [11] M. Zinkevich, Constitution of the Sr–Ni–O system, *J. Solid State Chem.* 178 (2005) 2818–2884, <https://doi.org/10.1016/j.jssc.2005.06.035>.
- [12] V. Vashook, J. Zosel, U. Guth, Oxygen solid electrolyte coulometry (OSEC), *J. Solid State Electrochem.* 16 (2012) 3401–3421, <https://doi.org/10.1007/s10008-012-1876-3>.
- [13] S.N. Ruddlesden, P. Popper, The compound Sr<sub>3</sub>Ti<sub>2</sub>O<sub>7</sub> and its structure, *Acta Crystallogr.* 11 (1958) 54–55, <https://doi.org/10.1107/S0365110X58000128>.
- [14] G. Blasse, Distortions in the Sr<sub>2</sub>TiO<sub>4</sub> and Sr<sub>3</sub>Ti<sub>2</sub>O<sub>7</sub> structures and their spectroscopic detection, *Chem. Phys. Lett.* 33 (1975) 616–618, [https://doi.org/10.1016/0009-2614\(75\)85787-3](https://doi.org/10.1016/0009-2614(75)85787-3).
- [15] D. Pelloquin, N. Barrier, A. Maignan, V. Caignaert, Reactivity in air of the Sr<sub>3</sub>Co<sub>2</sub>O<sub>7-δ</sub> RP = 2 phase: formation of the hydrated Sr<sub>3</sub>Co<sub>2</sub>O<sub>5</sub>(OH)<sub>2</sub>xH<sub>2</sub>O cobaltite, *Solid State Sci.* 7 (2005) 853–860, <https://doi.org/10.1016/j.solidstatesciences.2005.01.023>.
- [16] L.V. Makhnach, V.V. Pankov, P. Strobel, High-temperature oxygen non-stoichiometry, conductivity and structure in strontium-rich nickelates La<sub>2-x</sub>Sr<sub>x</sub>NiO<sub>4-δ</sub> (x = 1 and 1.4), *Mater. Chem. Phys.* 111 (2008) 125–130, <https://doi.org/10.1016/j.matchemphys.2008.03.022>.
- [17] J. Wan, J. Goodenough, J. Zhu, Nd<sub>2-x</sub>La<sub>x</sub>NiO<sub>4+δ</sub>, a mixed ionic/electronic conductor with interstitial oxygen, as a cathode material, *Solid State Ionics* 178 (2007) 281–286, <https://doi.org/10.1016/j.ssi.2007.01.013>.
- [18] V.V. Vashook, I.I. Yushkevich, L.V. Kokhanovsky, L.V. Makhnach, S.P. Tolochko, I.F. Kononyuk, H. Ullmann, H. Altenburg, Compositions and conductivity of some nickelates, *Solid State Ionics* 119 (1999) 23–30, [https://doi.org/10.1016/S0167-2738\(98\)00478-0](https://doi.org/10.1016/S0167-2738(98)00478-0).
- [19] V.V. Vashook, S.P. Tolochko, I.I. Yushkevich, L.V. Makhnach, I.F. Kononyuk, H. Altenburg, H. Ullmann, Oxygen nonstoichiometry and electrical conductivity of the solid solutions La<sub>2-x</sub>Sr<sub>x</sub>NiO<sub>y</sub> (0 ≤ x ≤ 0.5), *Solid State Ionics* 110 (1998) 245–253, [https://doi.org/10.1016/S0167-2738\(98\)00134-9](https://doi.org/10.1016/S0167-2738(98)00134-9).
- [20] L. Samain, P. Amshoff, J.J. Biendicho, F. Tietz, A. Mahmoud, R.P. Hermann, S.Y. Istomin, J. Grins, G. Svensson, Crystal structure and high-temperature properties of the Ruddlesden–Popper phases Sr<sub>3-x</sub>Y<sub>x</sub>(Fe<sub>1.25</sub>Ni<sub>0.75</sub>)O<sub>7-δ</sub> (0 ≤ x ≤ 0.75), *J. Solid State Chem.* 227 (2015) 45–54, <https://doi.org/10.1016/j.jssc.2015.03.018>.